

Superconductivity, phase fluctuations and the c-axis conductivity of bilayer high temperature superconductors

N. Shah and A. J. Millis

Center for Materials Theory

Department of Physics & Astronomy, Rutgers University

136 Frelinghuysen Road, Piscataway, NJ 08854

We present a theory of the interplane conductivity of bilayer high temperature superconductors, focusing on the effect of quantal and thermal fluctuations on the oscillator strengths of the superfluid stiffness and the bilayer plasmon. We find that the opening of the superconducting gap and establishment of superconducting phase coherence each lead to redistribution of spectral weight over wide energy scales. The factor-of-two relation between the superfluid stiffness and the change below T_c in the oscillator strength of the absorptive part of the conductivity previously derived for single-layer systems, is found to be substantially modified in bilayer systems. PACS: 74.20-z, 74.25.Gz, 78.20.-e

I. INTRODUCTION

The interlayer ('c-axis') conductivity of high temperature superconductors is an important and long standing problem. Experimental results [1–5] have seemed to many workers [6–9] to be sharply at variance with conventional understanding and to imply the existence of radically new physics. Other workers, conversely, have argued that many aspects of the results can be understood in a straightforward manner [10]. Especially interesting have been apparent violations of the Ferrel-Glover-Tinkham sum rule [11] relating the superfluid stiffness to changes in the absorptive part of the conductivity as temperature is reduced below the transition temperature T_c .

Recently Ioffe and one of us [12,13] have argued that the interlayer conductivity is a theoretically simple object (basically the convolution of two in-plane Green functions) and is therefore a sensitive probe of in-plane scattering rates and of the quantal and thermal phase fluctuations characterizing the superconducting state. A number of predictions were made, some of which appear to agree with experiment and some of which do not [5]. The results reported in [12,13] had a crucial limitation: the equations were derived for a 'single-layer' system such as $La_{2-x}Sr_xCuO_4$, whereas most (but not all) of the experimentally studied systems (including $Bi_2Sr_2Ca_2Cu_2O_8$ and $YBa_2Cu_3O_{7-\delta}$) have a 'bilayer' structure, with a unit cell containing two superconducting CuO_2 planes coupled to each other more strongly than to the planes in adjoining unit cells. The new feature introduced by the bilayer structure is "local field corrections": application of a uniform field can lead to a non-uniform charge distribution within a unit cell, which in turn causes internal fields affecting the motion of charges. This leads to phenomena not found in single plane systems; for example, the bilayer plasmon feature observed and discussed by van der Marel and others [3]. Interest in this fea-

ture was recently increased by the observation [14] that the bilayer plasmon frequency may provide information about the in-plane electronic compressibility, a quantity of great theoretical interest not easily accessible by other techniques.

In this paper we generalize the treatment of [12,13] to the bilayer case. We provide a simple and physically transparent treatment of the c-axis conductivity in the limit (appropriate for the high temperature superconductors) in which the interplane coupling is weak relative to in-plane energy scales. Our treatment includes phonon, bilayer plasmon and quasiparticle absorption. Our results provide a justification for previously proposed phenomenological oscillator models and allow us to determine the interplay between bilayer plasmon features and interlayer phase coherence. Our methods may easily be generalized to more complicated situations such as the three and four layer structures found in other high- T_c materials, but this generalization is not given here.

The rest of this paper is organized as follows. In Sec II we present the formalism; Sec III gives results calculated in the absence of phonons; Sec IV discusses the spectral weight and sum-rule analysis. In Sec V we extend our treatment to incorporate phonons (relevant for some bilayer materials) and finally in Sec VI we summarize our conclusions and discuss the applications to experiment.

II. FORMALISM

A. Fundamental Equations

We study the bilayer system shown in Fig 1 in which each unit cell contains two conducting planes separated by a distance d_1 and coupled by a hopping t_1 . The distance between a plane in one unit cell and the closest conducting plane in another unit cell is d_2 , so the lattice parameter in the interplane direction is $d = d_1 + d_2$.

Planes separated by a distance d_2 are coupled by a hopping t_2 . We neglect further neighbor hoppings, although these can be easily added at the cost of increased complexity of our equations. In the high T_c context, $t_2 \ll t_1$ (but our results are valid for any ratio t_2/t_1) and both t_1 and t_2 depend strongly on in-plane momentum, being maximal for momenta in the $(0, \pi)$ region of the zone and minimal for momenta near the zone diagonals $(\pm\pi, \pm\pi)$. We will usually not write the momentum dependence explicitly.

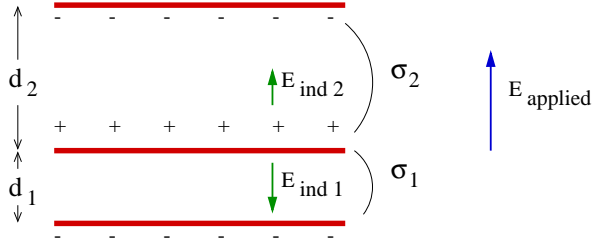


Fig. 1 Geometry considered in present paper. Shown is one unit cell (chosen as two close planes) and part of the next unit cell. The figure also shows the applied spatially uniform electric field ($E_{applied}$), the charge build-up on planes (represented as + + + and - - -) and the resultant induced fields $E_{ind1,2}$ which in turn affect the charge flow.

We refer to the two planes in one unit cell by the index $l = a, b$ and to the region between two planes separated by d_1 as region 1 and the region between two planes separated by d_2 as region 2; we label the unit cells by the index i . We take all planes to be identical and neglect all interplane couplings except for the hoppings and the internal electric fields induced by nonuniform charge distributions. We allow for the possibility that the planes are at different electrochemical potential μ . The Hamiltonian describing the system is then

$$H = \sum_{i,l} H_{in-plane} \quad (1)$$

$$- \sum_{i,\sigma} \int \frac{d^2p}{(2\pi)^2} t_1(p) \left(e^{i(\mu_{i,a} - \mu_{i,b})t} c_{i,a,p,\sigma}^+ c_{i,b,p,\sigma} + H.c. \right) -$$

$$\sum_{i,\sigma} \int \frac{d^2p}{(2\pi)^2} t_2(p) \left(e^{i(\mu_{i-1,b} - \mu_{i,a})t} c_{i-1,b,p,\sigma}^+ c_{i,a,p,\sigma} + H.c. \right),$$

where $H_{in-plane}$ (which we will not need to specify) describes the electronic physics within a CuO_2 plane. We shall study the properties of this Hamiltonian by a perturbation expansion in t_1 and t_2 . The dimensionless parameter is $t_{1,2}/E_{in-plane}$ where $E_{in-plane}$ is the in-plane density of states or inverse of some other important in-plane local energy scale. This approach has been shown to agree with results obtained by other means in a number of contexts, including coupled Luttinger liquids [15,16] and semiconductor heterostructures [17].

We are interested in optical experiments [2-5] which may be thought of as involving the application to the sys-

tem of a weak spatially uniform transverse electric field of magnitude E_T directed perpendicular to the planes. The experimentally determined quantity is the bilayer conductivity $\sigma_{bilayer}$, which is the coefficient relating the applied electric field to the spatial average of the current. The applied field leads to an electrochemical potential $\mu_{i,l}$ on each plane which has three contributions: from the applied electric field, from fields generated by build-up of charge on particular planes (shown as $E_{ind1,2}$ in Fig 1), and from changes in the in-plane chemical potential due to changes in the in-plane density. We have

$$\mu_{i,l} = eE_T R_{i,l} + eV_{ind}[\{n_{i',l'}\}] + \chi^{-1} n_{i,l}/e^2, \quad (2)$$

where $R_{i,l}$ is the position vector of the plane in the interplane direction and the zeros of charge density n and of chemical potential μ have been defined to correspond to the states of the planes in equilibrium. eV_{ind} is the electrochemical potential due to electric fields produced by charge build up and $\chi^{-1} = e\partial\mu/\partial n$ is inverse of the exact in-plane density-density correlation function of $H_{in-plane}$. The factors of e arise from converting particle densities to charge densities.

The spatially varying chemical potential leads to interplane electrical currents described by operators such as

$$j_{i,1} = -et_1 \sum_{\sigma} \int \frac{d^2p}{(2\pi)^2} (e^{ieV_{i,1}t} c_{i,a,p\sigma}^+ c_{i,b,p\sigma} - H.c.) \quad (3)$$

and therefore to interplane charge build-up, for which we must solve self consistently. In the present simple situation, application of a uniform electric field leads to two independent densities n_a and n_b and two independent chemical potential differences, $eV_1 = \mu_{i,a} - \mu_{i,b}$ and $eV_2 = \mu_{i-1,b} - \mu_{i,a}$. Combining the continuity equation for the current, the Maxwell equation and the density, and evaluating the currents to leading nontrivial order in $t_{1,2}$ and E_T leads to an expression for $\sigma_{bilayer}$. This expression is most conveniently written in terms of conductivities σ_1 (σ_2) appropriate to a ‘single-layer’ material consisting of an infinite stack of identical planes all separated by distance d_1 (d_2) and coupled by hopping t_1 (t_2) and is

$$\sigma_{bilayer}(\omega) = \frac{\sigma_1 \sigma_2 - i\omega(\sigma_1 \tilde{d}_1 + \sigma_2 \tilde{d}_2)/C}{\sigma_1 \tilde{d}_2 + \sigma_2 \tilde{d}_1 - i\omega/C} \quad (4)$$

with $\tilde{d}_{1,2} = d_{1,2}/(d_1 + d_2)$. Here the ‘blockade parameter’

$$C = \frac{4\pi}{\varepsilon} + \frac{2\chi d}{\varepsilon^2 d_1 d_2}, \quad (5)$$

where ε is the ‘background’ dielectric function due to non-electronic degrees of freedom. In this paper we shall take ε to be constant except in Sec V where we note include the effects of phonons (important in the optical absorption of some high- T_c materials) by using an $\varepsilon(\omega)$ with

appropriate frequency dependence in the expressions for $\sigma_{bilayer}$. The constant C expresses the blocking effects arising because charge which flows onto a plane via the strong link (large conductivity) will take a long time to flow off via the weak link: if the driving frequency is low, charge buildup will therefore occur, inhibiting additional motion of charge across the strong link.

Eq 4 reproduces all of the obvious limits correctly: as $\omega \rightarrow 0$ it reduces to $\sigma_{bilayer}^{-1} = \tilde{d}_2/\sigma_2 + \tilde{d}_1/\sigma_1$ so $\sigma_{bilayer}$ is dominated by smaller of the conductivities as expected, while if $\omega = C \text{Im}(\sigma_1(\omega)\tilde{d}_2 + \sigma_2(\omega)\tilde{d}_1)$ then a ‘bilayer plasmon’ pole occurs (damped, of course, by the dissipative part of the conductivity). If $d_1 = d_2$ and $\sigma_1 = \sigma_2$ then the system becomes effectively single-layered and Eq 4 shows $\sigma_{bilayer} = \sigma_1$.

The calculation of the constituent conductivities $\sigma_{1,2}$ is given in [12,13] and relevant results will be recalled in the next subsection. We note here that for consistency they (and χ^{-1}) must be calculated to leading nontrivial order in the interplane hoppings $t_{1,2}$. χ^{-1} is therefore a single-plane quantity and $\sigma_{1,2}$ may therefore be expressed in terms of convolutions of two-dimensional in-plane Green functions. If higher order expressions are used then for example, exchange interaction contributions must be included in C and further changes to $\sigma_{bilayer}$ will occur.

We see that the frequency dependence of the bilayer conductivity is complicated and depends on the value of C and on the magnitudes and frequency dependences of the individual conductivities. In general $\sigma_{bilayer}$ exhibits three regimes: a high frequency regime in which $\sigma_{bilayer} = \sigma_1\tilde{d}_1 + \sigma_2\tilde{d}_2$; a low frequency regime in which $\sigma_{bilayer} \approx \sigma_2/\tilde{d}_2$ and a broad crossover regime with characteristic scale

$$\omega^* = C \left| \sigma_1(\omega^*)\tilde{d}_2 + \sigma_2(\omega^*)\tilde{d}_1 \right| \quad (6)$$

which depends on the conductivities. If in the superconducting state, $\omega^* < 2\Delta$ then the scale ω^* becomes identical to the bilayer plasmon frequency $\omega_{bilayer}$ and near $\omega_{bilayer}$ we have

$$\sigma(\omega \sim \omega_{bilayer} < 2\Delta) = \frac{-i\rho_{bilayer}}{\omega - \omega_{bilayer} + i\delta} \quad (7)$$

defining the strength $\pi\rho_{bilayer}$ of the bilayer plasmon absorption.

B. Constituent conductivities

The calculation of the constituent conductivities is discussed at length in [12,13]. Here we briefly recall key results and needed formulae. The conductivities are given by correlation functions of current operators such as j_1 above and involve expectation values of the form $t^2(p) \langle c_{i,p}^+(t)c_{j,p}(t)c_{j,p}^+(t')c_{i,p}(t') \rangle$. To leading order in

t , correlations between operators on different planes vanish so the expression may be written as the sum of two terms, one involving $\langle c_{i,p}^+(t)c_{i,p}(t') \rangle \langle c_{j,p}^+(t')c_{j,p}(t) \rangle$ (i.e. the product of two ‘normal’ in-plane Green functions $G(p, t-t')$) and one involving $\langle c_{i,p}^+(t)c_{i,p}(t') \rangle \langle c_{j,p}(t')c_{j,p}(t) \rangle$ (i.e. the product of two ‘anomalous’ in-plane Green functions $F(p, t-t')$). However, the anomalous Green function involves the superconducting order parameter which has a phase which we denote by ϕ . The product of anomalous Green functions on planes i and j therefore involves the factor $e^{i(\phi_i(r,t) - \phi_j(r',t'))}$ (times a short ranged function of r, t which depends on the details of the interplane hopping and the underlying energy scales of the superconductivity) and must be averaged over an ensemble describing the phase fluctuations. Refs [12,13] showed that in the case of interest here, these effects may be accounted for by multiplying the $F - F^+$ contribution to σ by a Debye-Waller factor α which is unity for a mean-field BCS superconductor with no fluctuations, may be reduced from unity by quantal or thermal fluctuations about an ordered state, and which becomes very small if there is no long range phase order. We follow refs [12,13] in assuming that the pseudogap state is characterized by a conventional superconducting gap but no interplane phase coherence.

Thus ($\nu = 1, 2$ labels planes)

$$\sigma_\nu(i\omega_n) = \frac{K_\nu + \Pi_\nu}{i\omega} \quad (8)$$

with the diamagnetic contribution given by

$$K_\nu = 4e^2d_\nu T \sum_n \int \frac{d^2p}{(2\pi)^2} t_\nu(p)^2 \left(-G(p, \omega'_n)G(p, \omega'_n) + \alpha F(p, \omega'_n)F(p, \omega'_n) \right) \quad (9)$$

and the paramagnetic contribution given by

$$\Pi_\nu = 4e^2d_\nu T \sum_n \int \frac{d^2p}{(2\pi)^2} t_\nu(p)^2 \left(G(p, \omega_n + \omega'_n)G(p, \omega'_n) + \alpha F(p, \omega_n + \omega'_n)F(p, \omega'_n) \right). \quad (10)$$

where G, F are the exact normal and anomalous Green functions corresponding to $H_{in-plane}$.

The $\omega \rightarrow 0$ limit is $\sigma \rightarrow \frac{i\rho_s}{\omega}$ with

$$\rho_{s,\nu} = 8\alpha e^2d_\nu T \sum_n \int \frac{d^2p}{(2\pi)^2} t_\nu(p)^2 F(p, \omega'_n)F(p, \omega'_n) \quad (11)$$

while the usual ‘f-sum rule’ arguments [18] yield ($\sigma^{(1)}$ is the absorptive part of the conductivity)

$$K = \int_0^\infty \frac{2d\omega}{\pi} \sigma^{(1)}(\omega) = \rho_s + \int_{0^+}^\infty \frac{2d\omega}{\pi} \sigma^{(1)}(\omega) \quad (12)$$

(note that in the first equality the integral is only over one half of the delta function at $\omega = 0$).

In the high- T_c materials the anisotropy of $t(p)$ is such that the interplane conductivity is dominated by the ‘‘corner’’ regions around $(0, \pi)$ and so we follow refs [12,13] and neglect both the angular variation of the gap and of $t_{1,2}$. In this approximation σ_1 and σ_2 have the same frequency dependence and differ only by a prefactor involving the square of the relevant hopping.

In high- T_c materials, the normal state c-axis conductivity is characterized by a very broad Drude-like absorption, corresponding to an in-plane Green function (in the ‘‘corner region’’) characterized by a very large, essentially frequency independent scattering rate. We therefore follow refs [12,13] and use this ‘dirty-limit’ form to compute the conductivities. We note that there is a large and growing literature on changes to the Green function as the temperature is changed through the superconducting transition [19–21]. The implication of these changes for the c-axis conductivity has been studied by [13], but because our main interest here is in the new features introduced by the bilayer structure and because there is no consensus on the physical origin or mathematical form of the superconductivity-induced changes, we do not consider them here. Further, we shall be interested mainly in three situations—the normal state, at a temperature well above the ‘pseudogap formation temperature’, the $T \rightarrow 0$ limit in the superconducting state, and temperatures well below the pseudogap scale and near to T_c , i.e. $T_c < T \ll \Delta$. Thus we may neglect the temperature, except as it influences the value of the Debye-Waller parameter α . We therefore have

$$\sigma_\nu^{(1)}(\omega) = -\sigma_{0,\nu}\Theta(|\omega| - 2\Delta) \quad (13)$$

$$\int_{\Delta}^{|\omega|-\Delta} \frac{\omega'(\omega' - |\omega|) + \alpha_\nu \Delta^2}{\sqrt{\omega'^2 - \Delta^2} \sqrt{(\omega' - |\omega|)^2 - \Delta^2}} \frac{d\omega'}{|\omega|}$$

$$\sigma_\nu^{(2)}(\omega) = \frac{\Delta(\alpha_\nu - 1)\pi}{2|\omega|} + \sigma_{0,\nu} \text{sgn}(\omega)\Theta(2\Delta - |\omega|) \quad (14)$$

$$\int_{\Delta}^{|\omega|+\Delta} \frac{\omega'(\omega' - |\omega|) + \alpha_\nu \Delta^2}{\sqrt{\omega'^2 - \Delta^2} \sqrt{\Delta^2 - (\omega' - |\omega|)^2}} \frac{d\omega'}{|\omega|}$$

$$+ \sigma_{0,\nu} \text{sgn}(\omega)\Theta(|\omega| - 2\Delta)$$

$$\int_{|\omega|-\Delta}^{|\omega|+\Delta} \frac{\omega'(\omega' - |\omega|) + \alpha_\nu \Delta^2}{\sqrt{\omega'^2 - \Delta^2} \sqrt{\Delta^2 - (\omega' - |\omega|)^2}} \frac{d\omega'}{|\omega|}$$

with $\sigma_{0,\nu}$ the normal state (neither superconductivity nor any gap) conductivity, frequency independent because we have taken the dirty limit. We note that because $t_{1,2}$ differ, so also may the quantum fluctuation parameters $\alpha_{1,2}$. The considerations of [13] suggest that α is dominated by in-plane fluctuations, so may not differ much between the two links, so in the rest of this paper we set $\alpha_1 = \alpha_2$.

The single-layer superfluid stiffnesses following from these expressions are

$$\rho_{s,\nu} = \alpha_\nu \rho_{s,\nu}^{BCS} = \alpha_\nu \pi \sigma_{0,\nu} \Delta, \quad (15)$$

where $\rho_{s,\nu}^{BCS}$ is the superfluid stiffness following from the assumption of full phase coherence ($\alpha_\nu = 1$).

III. CALCULATED CONDUCTIVITY

In this section we evaluate the formulas derived in the previous section. The fundamental result was Eq 4, which expressed the conductivity $\sigma_{bilayer}$ of a bilayer system in terms of the conductivities $\sigma_{1,2}$ of effective ‘single-layer’ systems corresponding to the two interplane spacings of the bilayer and a ‘‘blockade parameter’’ C expressing interplane interaction effects. We use the normal state ($\Delta = 0$) value of the characteristic frequency scale ω^* defined by Eq 6,

$$\omega^* = C \sigma_{0,1} \tilde{d}_2 \left(1 + \frac{\sigma_{0,2} \tilde{d}_1}{\sigma_{0,1} \tilde{d}_2} \right), \quad (16)$$

in our discussion henceforth. It is most convenient to express C in terms of this normal state value of ω^* .

The important dimensionless parameters are the ratio of normal state conductivities $b = \sigma_{0,2}/\sigma_{0,1} < 1$, ω^*/Δ and the Debye-Waller factors $\alpha_{1,2}$ introduced above Eq 8. To simplify the presentation of our results, we define conductivity units such that $\sigma_{0,1} = 1$ and frequency units such that $\Delta = 1$. For definiteness we choose the normalized interplane distances to be $\tilde{d}_1 = 0.4$, $\tilde{d}_2 = 0.6$ so $\omega^* = 0.6\sigma_{0,1}C(1 + 2b/3)$. and set $\alpha_1 = \alpha_2$.

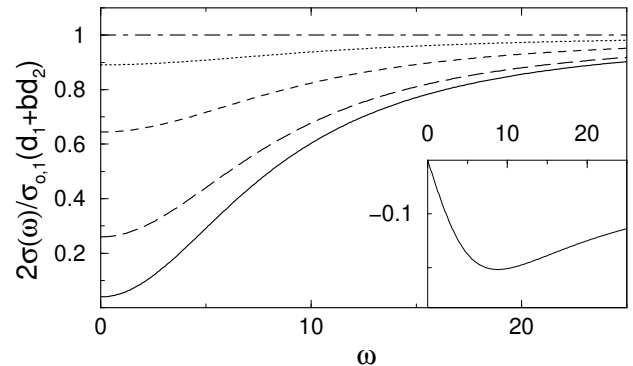


Fig. 2 Real part of normal state conductivity scaled by $\sigma_{0,1}(\tilde{d}_1 + b\tilde{d}_2)$ for $b = 1, 0.5, 0.25, 0.075, 0.01$ (from top to bottom). The bilayer frequency $\omega^* = 11.48, 9.91, 8.8, 8.39$ for $b = 0.5, 0.25, 0.075, 0.01$, respectively. The inset shows imaginary part of the conductivity for $b = 0.075$.

Fig 2 shows the real part of the normal state conductivity for the five values $b = 1, 0.5, 0.25, 0.075, 0.01$. The suppression of the low frequency conductivity by the blockade effect is evident, as is the gradual crossover to the high frequency isolated layers value. The curves have been scaled by $\sigma_{0,1}(\tilde{d}_1 + b\tilde{d}_2)$ so that all have the same high frequency limit. The inset shows the imaginary part

for $b = 0.075$. In the crossover regime, the blockade effect is seen to lead to out of phase response.

We now consider the superconductivity induced changes. The top panel of Fig 3 shows the result of evaluating Eq 4 in the ‘single-layer’ ($b = 1$) fully phase coherent ($\alpha_\nu = 1$) case. The opening of the superconducting gap suppresses the real part of the conductivity for frequencies below 2Δ and changes the form somewhat for $\omega \gtrsim 2\Delta$. The establishing of superconducting phase coherence leads to a divergent low frequency response characterized by the superfluid stiffness $\rho_{s,bilayer}$. The oscillator strength in the superfluid response is shown in the top panel as a shaded rectangle. The f-sum rule arguments discussed at length in the next section imply that in the fully phase coherent ($\alpha_\nu = 1$) case, the area lost in the absorptive part of σ due to the opening of the superconducting gap is transferred to the superfluid response. It is apparent from the figure that the area in the shaded rectangle is approximately equal to the ‘missing’ area and we have verified numerically that the areas are equal: $\int_0^\infty d\omega[\sigma(\Delta = 0) - \sigma(\Delta)] = \pi\rho_{s,bilayer}/2$.

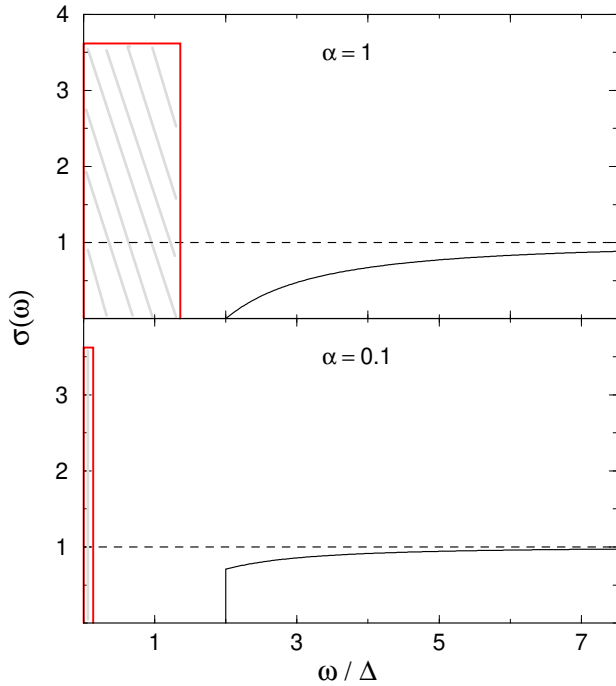


Fig. 3 Real part of conductivity for ‘single-layer’ ($b = 1$) system. Top panel corresponds to fully phase coherent ($\alpha_\nu = 1$) while the bottom panel to $\alpha_\nu = 0.1$ superconducting state. The dashed line in both corresponds to the normal state. The area of the shaded rectangle equals $\pi\rho_s/2$ in each case.

If $b < 1$ then the situation is much more involved. In particular because the form of the conductivity in the regime $\omega \sim \omega^*$ depends sensitively on the interplay between C and $\sigma_{1,2}$, the superconductivity induced changes in $\sigma_{1,2}$ will lead to large changes in $\sigma_{bilayer}$. In addition, some of the oscillator strength eliminated from the

$\omega < 2\Delta$ region by the opening of the gap will go into the bilayer plasmon absorption instead of into the superfluid delta function.

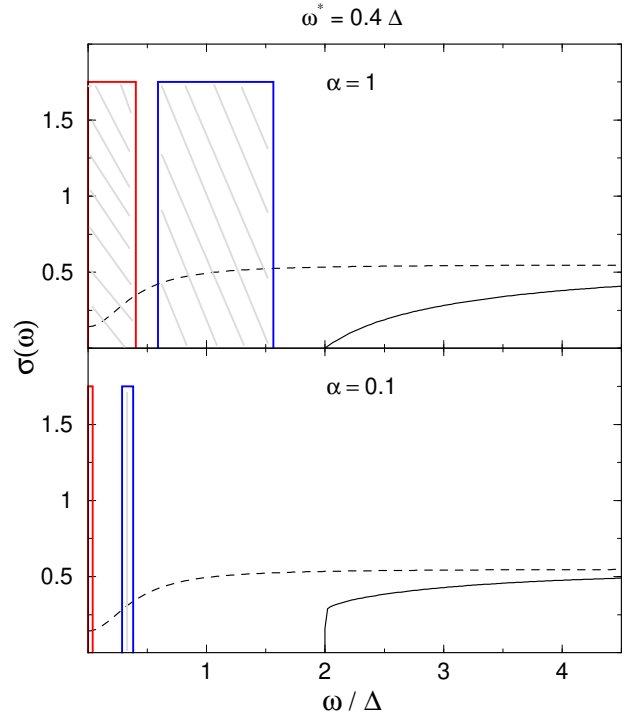


Fig. 4 Real part of conductivity for bilayer ($b = 0.075$) system for $\omega^* = 0.4\Delta$. Top panel corresponds to fully phase coherent ($\alpha_\nu = 1$) and bottom panel to $\alpha_\nu = 0.1$ superconducting state. The dashed line in both corresponds to the normal state conductivity. The area of the two shaded rectangles in each panel equals $\pi\rho_s/2$ and $\pi\rho_{bilayer}$ for rectangles centered at $\omega = 0$ and $\omega_{bilayer}$, respectively.

The top panels of Figs 4, 5 and 6 show the normal and superconducting state conductivity in the fully phase coherent ($\alpha_\nu = 1$) limit for three representative values of ω^* : 0.4Δ , 3Δ and 10Δ , respectively in the strongly anisotropic limit $b = 0.075$. The oscillator strengths in the superfluid response and (if it is inside the gap) the bilayer plasmon are shown as shaded rectangles. For $\omega^* = 0.4\Delta$, the bilayer plasmon lies within the superconducting gap. The resulting absorption is a delta function at the marked frequency, with an intensity corresponding to an integrated area equal to that of the rectangular box shown. For $\omega^* = 3\Delta$ the bilayer plasmon lies just above the gap, visible as a sharp feature at the gap edge and the remainder of the superconducting conductivity is slightly suppressed over a wide frequency range. For $\omega^* = 10\Delta$ the bilayer plasmon feature is evident only as a very broad absorption at frequencies that are much larger than shown here.

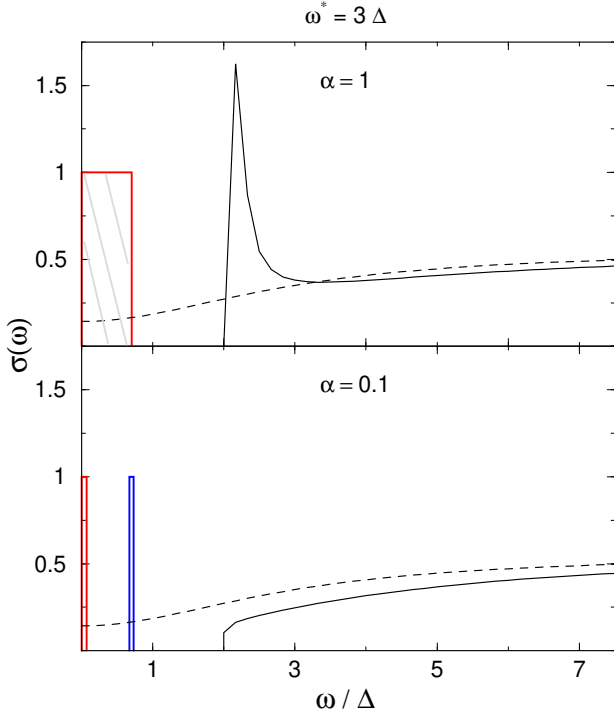


Fig. 5 Real part of conductivity for bilayer ($b = 0.075$) system for $\omega^* = 3\Delta$. Top panel corresponds to fully phase coherent ($\alpha_\nu = 1$) and bottom panel to $\alpha_\nu = 0.1$ superconducting state. The dashed line in both corresponds to the normal state conductivity. The area of the shaded rectangle at $\omega = 0$ in each panel equals $\pi\rho_s/s$ while the area of the rectangle at $\omega_{bilayer}$ in the second panel equals $\pi\rho_{bilayer}$.

The bottom panels of Figs 4, 5 and 6 show the effect of phase fluctuations, displaying the superconducting curves for the same ω^* and b values as the respective top panels, but with $\alpha_\nu = 0.1$. For $\omega > 2\Delta$ the difference between the normal and the superconducting conductivity increases as phase fluctuations become more important. Both the strength and the frequency of the bilayer plasmon feature depend strongly on the value of the fluctuation parameter. For $\omega^* = 3\Delta, 10\Delta$, the bilayer plasmon moves below the gap as seen in Figs 5 and 6. For the pseudogap case ($\alpha_\nu = 0$) both the bilayer plasmon and the superconducting delta function are absent and the $\omega > 2\Delta$ conductivity is roughly the same as the $\alpha_\nu = 0.1$ case. We can also study the conductivity for different values of α_1 and α_2 and it is worth noting that in the case when $\alpha_2 = 0$ and $\alpha_1 \neq 0$, it is possible to get a bilayer plasmon feature though the superconducting delta function is absent.

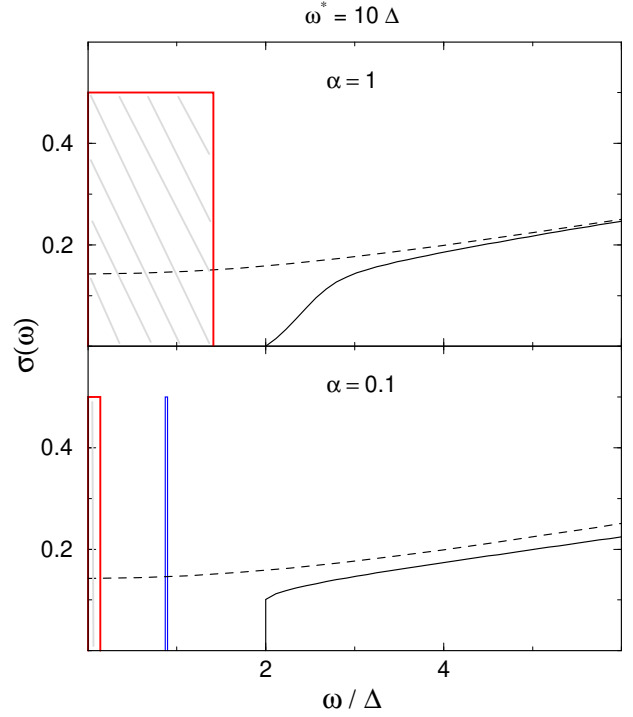


Fig. 6 Real part of conductivity for bilayer ($b = 0.075$) system for $\omega^* = 10\Delta$. Top panel corresponds to fully phase coherent ($\alpha_\nu = 1$) and bottom panel to $\alpha_\nu = 0.1$ superconducting state. The dashed line in both corresponds to the normal state conductivity. The area of the shaded rectangle at $\omega = 0$ in each panel equals $\pi\rho_s/s$ while the area of the rectangle at $\omega_{bilayer}$ in the second panel equals $\pi\rho_{bilayer}$.

Fig 7 plot the bilayer plasmon frequency $\omega_{bilayer}$, the spectral weight in the bilayer plasmon $\rho_{bilayer}$ (defined by Eq 7) and the spectral weight in the superconducting delta function (at $\omega = 0$) ρ_s as a function of $\alpha_1 = \alpha_2$ for $b = 0.1$ and $\omega^* = 0.4\Delta$. The two spectral weights vary linearly in the fluctuation parameter for the given value of ω^* and hence their ratio is independent of the α_ν value.

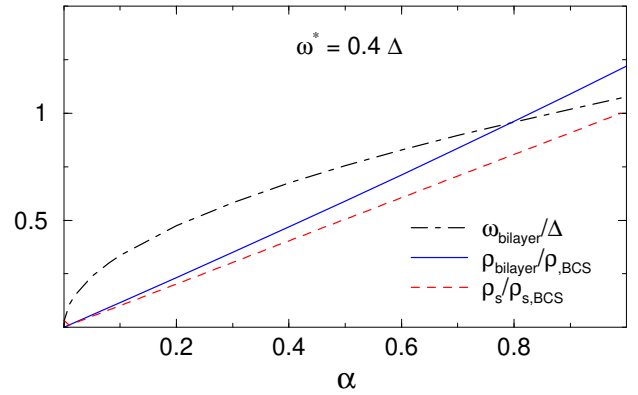


Fig. 7 The bilayer plasmon frequency $\omega_{bilayer}$, the spectral weight in the bilayer plasmon $\rho_{bilayer}$ (defined by Eq 7) and the spectral weight in the superconducting delta function (at $\omega = 0$)

ρ_s as a function of $\alpha_1 = \alpha_2$ for $b = 0.075$ and $\omega^* = 0.4\Delta$.

IV. SUPERFLUID STIFFNESS AND SUM RULES

At very low frequencies in the superconducting state one has

$$\sigma_{bilayer} \rightarrow \frac{i\rho_{s,bilayer}}{\omega}. \quad (17)$$

Inspection of Eq 4 shows that

$$\rho_{s,bilayer} = \frac{\rho_{s,1}\rho_{s,2}}{\rho_{s,1}\tilde{d}_2 + \rho_{s,2}\tilde{d}_1} = \pi\sigma_{0,1}\Delta \frac{b\alpha_1\alpha_2}{\alpha_1\tilde{d}_2 + b\alpha_2\tilde{d}_1}, \quad (18)$$

where the first equation applies to all bilayer systems and the second follows from the specific assumptions we have made. One question of current experimental interest is the relation between the superfluid stiffness and changes in conductivity as the temperature is reduced (a) below the ‘pseudogap’ scale at which the gap opens and (b) below T_c at which phase coherence is established. In Refs [12,13] these relations were established for the ‘single-layer’ case. The numerical results presented in the previous section show that differences occur in the bilayer case. To analyze this issue more precisely, we note that the dirty-limit model analyzed in this paper should be viewed as arising from a model with a very large but finite scattering rate Γ in the limit $(\Omega, \Omega_{bilayer}, \Delta) \ll \Gamma$. The standard sum rule derivations are based on analysis of the $\Omega/\Gamma \rightarrow \infty$ limit. However, one may obtain sum rules for the superconductivity and pseudogap induced changes in σ without considering this limit. We define the change in the spectral weight as Δ is increased from $\Delta = 0$ by

$$\delta K(\Omega, \Delta, \alpha) = \int_0^\Omega \frac{2d\omega}{\pi} [\sigma(\Delta, \alpha) - \sigma(\Delta = 0)]. \quad (19)$$

This quantity remains finite in the limit $\Omega \rightarrow \infty$, $\Omega/\Gamma \ll 1$. The values we obtain with our $\Gamma \rightarrow \infty$ limit are accurate up to terms of relative order $(\Omega_{bilayer}, \Delta)/\Gamma$.

It is also useful to consider the change in the spectral weight excluding the superfluid response : we define

$$\begin{aligned} \delta K_+(\Omega, \Delta, \alpha) &= \int_{0^+}^\Omega \frac{2d\omega}{\pi} [\sigma(\Delta, \alpha) - \sigma(\Delta = 0)] \\ &= \delta K(\Omega, \Delta, \alpha) - \rho_s(\Delta, \alpha) \end{aligned} \quad (20)$$

and the ratio of change in δK_+ with α to the superfluid stiffness given by

$$R(\Omega) = \frac{\delta K_+(\Omega, \Delta, \alpha) - \delta K_+(\Omega, \Delta, 0)}{\rho_s(\Delta, \alpha)}. \quad (21)$$

Now Refs [12,13] showed that for a ‘single-layer’(s-l) system, the change in the spectral weight as defined by Eq 19 is

$$\delta K_{s-l}(\Omega = \infty, \Delta, \alpha) = -\frac{(1-\alpha)\rho_s^{BCS}(\Delta)}{2}, \quad (22)$$

where $\rho_s^{BCS}(\Delta)$ is defined by Eq 15. Thus the change with α in total spectral weight at fixed Δ is

$$\begin{aligned} \delta K_{s-l}(\Omega = \infty, \Delta, \alpha) - \delta K_{s-l}(\Omega = \infty, \Delta, 0) \\ = \frac{\alpha\rho_s^{BCS}(\Delta)}{2} \end{aligned} \quad (23)$$

and the change with α in the $\Omega > 0$ spectral weight as defined by Eq 20 is

$$\begin{aligned} \delta K_{+,s-l}(\Omega = \infty, \Delta, \alpha) - \delta K_{+,s-l}(\Omega = \infty, \Delta, 0) \\ = -\frac{\alpha\rho_s^{BCS}(\Delta)}{2} = -\frac{\rho_s^{s-l}(\Delta, \alpha)}{2} \end{aligned} \quad (24)$$

Use of Eq. 21 gives the value of $R_{s-l}(\Omega = \infty) = -1/2$. In other words, if the superconducting gap appears without phase coherence, the oscillator strength decreases by an amount related to the ‘BCS’ superfluid stiffness, essentially because the conductivity in the region less than the gap is suppressed and no additional oscillator strength appears in the superfluid response. If phase coherence is now turned on, the total oscillator strength and the superfluid stiffness increase, while the spectral weight in the $\Omega > 0$ conductivity decreases. Comparison of Eq 14 and Eq 23 shows that in the ‘single-layer’ case the ratio between these changes is 2:1.

Applying these arguments to the bilayer case shows that

$$\delta K_{bilayer}(\Omega = \infty, \Delta, \alpha_\nu) = -\frac{1}{2} \sum_\nu (1 - \alpha_\nu) \pi \sigma_{0,\nu} \tilde{d}_\nu \Delta. \quad (25)$$

The simple factor-of-two relation between the phase-coherence-induced change in δK_+ and the superfluid stiffness does not occur in the bilayer system essentially because when the phase coherence parameter is varied, the strengths of both the bilayer plasmon feature and the superfluid stiffness vary. To see what the relation is, we plot in Fig 8 the ratio $R_{bilayer}(\Omega = \infty)$ as a function of bilayer anisotropy b ($R_{bilayer}(\Omega = \infty)$ being independent of $\alpha_1 = \alpha_2 = \alpha$). We see that the ratio increases monotonically as b is decreased from the single-layer value $b = 1$, and changes sign at a d_1/d_2 dependent value of $b \sim 0.2$. Thus unlike in the single-layer case, where ρ_s increased by twice the decrease in $\delta K_+(\Omega = \infty)$, in the bilayer case the increase is generically greater than $2\delta K_+(\Omega = \infty)$ and indeed for extreme anisotropy both $\delta K_+(\Omega = \infty)$ and ρ_s increase as α is increased from zero.

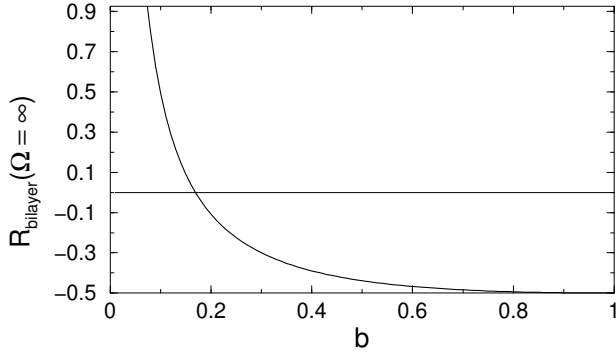


Fig. 8 Ratio of the change in δK_+ on onset of phase coherence to the superfluid stiffness defined by Eq 21, $R_{bilayer}(\Omega = \infty)$ as a function of the anisotropy parameter b . Note that the ratio is independent of the value of α and that the $b = 1$ value corresponds to the single-layer case.

Fig 9 plots $R_{bilayer}$ as a function of the cut-off Ω . The $\Omega = \infty$ value is indicated by an arrow. We have verified that the calculated quantity does indeed converge to the correct $\Omega \rightarrow \infty$ value, but as can be seen, the convergence is very slow.

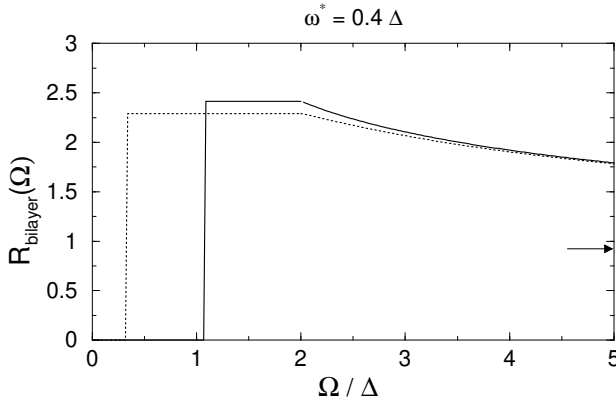


Fig. 9 Ratio of the change in δK_+ on onset of phase coherence to the superfluid stiffness defined by Eq 21, $R_{bilayer}$ plotted as a function of cut-off Ω for a bilayer ($b = 0.075$) system with $\omega^* = 0.4\Delta$. Solid line: fully phase coherent ($\alpha_\nu = 1$) superconducting state; dotted line: $\alpha_\nu = 0.1$ superconducting state. Arrow: $R_{bilayer}(\Omega = \infty)$.

Fig 10 shows the changes in spectral weight for the case of a large difference in interplane hopping ($b = 0.075$) and for $\omega^* = 0.4\Delta$ as a function of the cut-off frequency Ω . For $\alpha = 1$ (top panel), we expect conservation of the total spectral weight while for $\alpha = 0.1$ (bottom panel) we expect the $\Omega \rightarrow \infty$ value to be non-zero as given by Eq 25. A remarkably slow convergence of the change in the spectral weight to its $\Omega \rightarrow \infty$ value is evident. We verify the $\Omega \rightarrow \infty$ values numerically by plotting in Fig 11, $\delta K_{bilayer}$ as a function of inverse cut-off frequency. We have verified that the $1/\Omega \rightarrow 0$ limit matches the value given by Eq 25. Considerable caution must be exercised in the experimental investigations of changes in the spec-

tral weight because small differences persisting over wide frequency ranges may lead to appreciable contributions to sum rules.

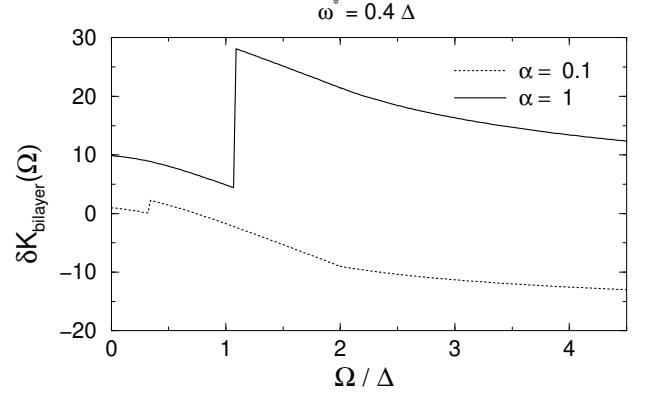


Fig. 10 $\delta K_{bilayer}$ (defined by Eq 19) as a function of cut-off frequency Ω for bilayer ($b = 0.075$) system for $\omega^* = 0.4\Delta$. Solid line corresponds to fully phase coherent ($\alpha_\nu = 1$) and dotted line to $\alpha_\nu = 0.1$ superconducting state.

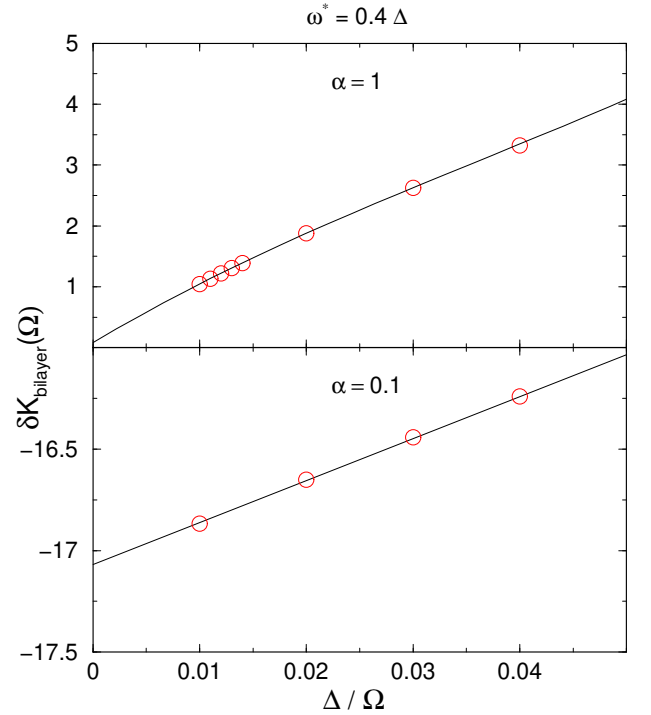


Fig. 11 $\delta K_{bilayer}$ as a function of inverse cut-off frequency Ω demonstrating convergence to correct sum-rule value. The $1/\Omega = 0$ value correctly gives the $\Omega \rightarrow \infty$ value as given by Eq 25. Top panel corresponds to fully phase coherent ($\alpha_\nu = 1$) and bottom panel to $\alpha_\nu = 0.1$ superconducting state.

V. INCLUSION OF PHONONS

Due to the proximity of the bilayer feature to the optical phonons in high- T_c materials like $Bi_2Sr_2Ca_2Cu_2O_8$ and $YBa_2Cu_3O_{7-\delta}$, it is of interest to study the interplay of phonons and the bilayer plasmon. In the first part of this paper we had taken $\varepsilon_1 = \varepsilon_2 = \varepsilon_\infty = \text{const.}$ To incorporate phonon modes we include in our analysis frequency dependent dielectric functions for each layer: $\varepsilon_1(\omega)$ and $\varepsilon_2(\omega)$. We obtain for interplane bilayer conductivity,

$$\sigma_{bilayer}^{phonon}(\omega) = \frac{\sigma_1\sigma_2 - \frac{i\omega}{4\pi}(\sigma_1(\varepsilon_2 - \tilde{d}_2) + \sigma_2(\varepsilon_1 - \tilde{d}_1))}{\sigma_1\tilde{d}_2 + \sigma_2\tilde{d}_1 - \frac{i\omega}{4\pi}(\varepsilon_1\tilde{d}_2 + \varepsilon_2\tilde{d}_1)} - \frac{\frac{\omega^2}{16\pi^2}(\varepsilon_1\varepsilon_2 - (\varepsilon_1\tilde{d}_2 + \varepsilon_2\tilde{d}_1))}{\sigma_1\tilde{d}_2 + \sigma_2\tilde{d}_1 - \frac{i\omega}{4\pi}(\varepsilon_1\tilde{d}_2 + \varepsilon_2\tilde{d}_1)}. \quad (26)$$

This more general formula reduces to Eq 4 with a value of $C = 4\pi/\varepsilon$ on choosing $\varepsilon_1 = \varepsilon_2 = \text{constant}$ (inclusion of the compressibility term χ leads to more complicated formulae).

To study the qualitative effect of including phonons we consider the simplest possible case of $\varepsilon_2 = 1$ and

$$\varepsilon_1(\omega) = \varepsilon_\infty + \frac{(\varepsilon_0 - \varepsilon_\infty)\omega_p^2}{\omega_p^2 - \omega^2 - i\omega\gamma}. \quad (27)$$

where ω_p is the frequency of the phonon mode and γ the broadening.

Fig. 12 displays the effects of adding, to the situation (full phase coherence ($\alpha = 1$) and bilayer plasmon inside the gap) shown in the top panel of Fig 4, a phonon with a frequency greater than the bilayer plasmon frequency. For orientation, the top panel shows the bilayer plasmon part of the electronic absorption in the absence of phonons (calculated from Eq.26 with $\varepsilon_1 = \varepsilon_2 = 1$), and the phonon absorption in the absence of electrons (calculated from Eq. 26 with $\sigma_1 = \sigma_2 = 0$). The bilayer plasmon was represented in Fig 4 as a rectangle and is shown here with a Lorentzian broadening. The phonon feature is rendered optically active and shifted up from the phonon frequency ω_p by bilayer effects. The lower panel of Fig 12 shows the full conductivity. The electronic continuum contribution at $\omega > 2\Delta$ is present but very difficult to perceive on the scale of this plot. It is evident that the coupling between the modes leads as usual to level repulsion, and that further, almost all of the oscillator strength goes into the upper mode. The lower mode (shown in expanded view in the inset) is almost invisible.

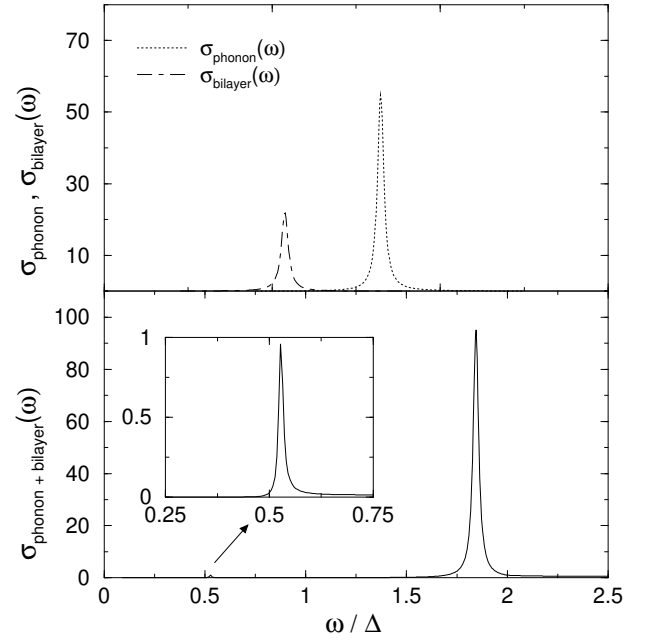


Fig. 12 Top panel plots the conductivity $\sigma_{phonon}(\omega)$ with $\omega_p = 0.91\Delta$ obtained from Eq 26 by putting the electron conductivities $\sigma_{1,2} = 0$ (dotted line) and the broadened bilayer conductivity $\sigma_{bilayer}(\omega)$ with $\omega^* = 0.4\Delta$ and $b = 0.075$ (dot-dashed line). The bottom panel plots $\sigma_{bilayer}^{phonon}(\omega)$ (Eq 26). The inset shows the lower peak not visible on the scale of the plot.

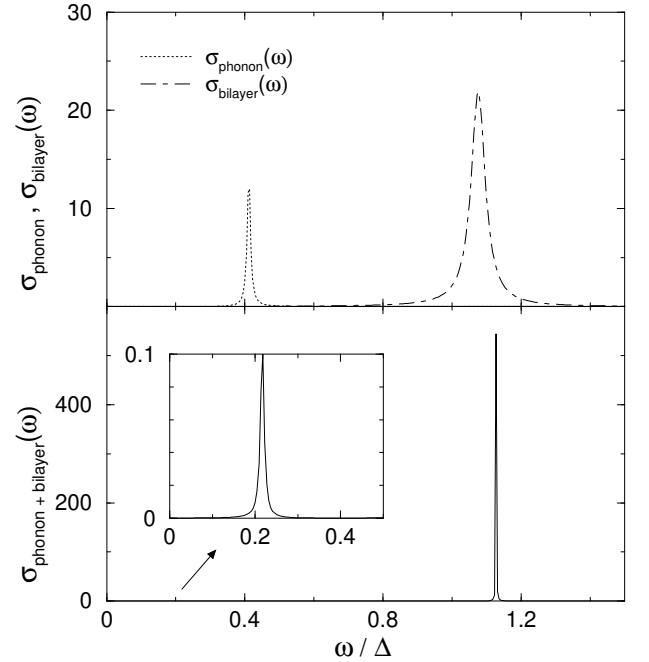


Fig. 13 Top panel plots the conductivity $\sigma_{phonon}(\omega)$ with $\omega_p \sim 0.23\Delta$ obtained from Eq 26 by putting the electron conductivities $\sigma_{1,2} = 0$ (dotted line) and the broadened bilayer conductivity $\sigma_{bilayer}(\omega)$ with $\omega^* = 0.4\Delta$ and $b = 0.075$ (dot-dashed line). The bottom panel plots $\sigma_{bilayer}^{phonon}(\omega)$ (Eq 26). The inset shows the lower peak not visible on the scale of the plot.

Fig. 13 shows that roughly the same situation is obtained if the phonon starts out at a lower frequency than the bilayer plasmon. In this case the upper mode shifts by rather less, but the qualitative features are the same.

We now briefly outline the effects of increasing phase fluctuations (decreasing α from unity) i.e increasing temperature. As can be seen from Figs 4-6, increasing phase fluctuations decreases the frequency and oscillator strength of the bilayer plasmon mode. Thus if the ‘bare’ phonon frequency is greater than the bilayer plasmon frequency (as in Fig 12), then relatively minor changes occur in the absorption spectrum as α is decreased. Essentially, the almost invisible lower absorption moves to the left and becomes a bit sharper which in turn results in the slight decrease in frequency and intensity of the upper absorption.

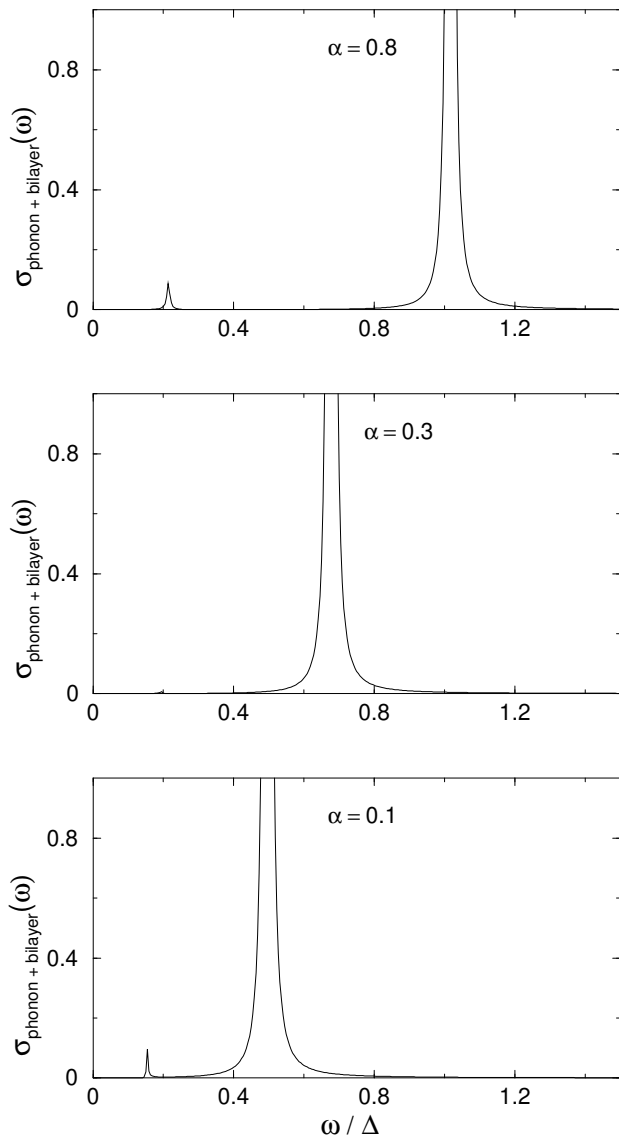


Fig. 14 The figure plots $\sigma_{bilayer}^{phonon}(\omega)$ (Eq 26) for $\alpha = 0.8$ (top panel), $\alpha = 0.3$ (panel two) and $\alpha = 0.1$ (bottom panel) for the same set of parameters as in Fig 13 ($\omega_p \sim 0.23\Delta$ $\omega^* = 0.4\Delta$).

On the other hand, if the $\alpha = 1$ bilayer plasmon is at a higher frequency than the phonon, more drastic changes will occur as shown in Fig 14. Decreasing α slightly results in a decrease in frequency and intensity of the stronger upper absorption as shown in the top panel of Fig 14 for $\alpha = 0.8$. As α is further decreased α the $\sigma_{bilayer}$ peak in Fig 13 goes on moving to the left and eventually overlaps with the σ_{phonon} peak at which point the lower absorption is almost invisible and the conductivity is as shown in the second panel of Fig 14 for $\alpha = 0.3$. On further decreasing α the $\sigma_{bilayer}$ peak crosses over to the left of σ_{phonon} and the conductivity is as given by the bottom panel of Fig 14 for $\alpha = 0.1$. Also note that the decrease in intensity of the upper peak is much stronger with the decrease in α as compared to the case when the ‘bare’ phonon frequency is greater than the bilayer plasmon frequency. From experimental point of view, the behavior of the observed peaks as a function of temperature might allow us to distinguish between the two situations where the ‘bare’ phonon frequency is greater than or smaller than the bilayer plasmon frequency.

Finally, we note that the spectral weight in the superfluid stiffness is unaffected by the phonons.

VI. CONCLUSIONS AND APPLICATIONS TO EXPERIMENT

We have extended the theory of refs [12,13] to the bilayer situation of relevance to many experimentally studied high- T_c materials. The crucial physics is local-field or ‘blockade’ effects: the difference in hopping amplitudes characteristic of a bilayer structure leads to charge imbalances inside the unit cell; the electrochemical potentials due to these charge imbalances act to suppress the low frequency response to a uniform electric field, and lead to bilayer plasmon features in the absorption. For the physics of high- T the crucial question is the observability of the effects of thermal and quantal fluctuations of the phase of the superconducting order parameter, here parameterized by a ‘Debye-Waller parameter α ’

We find a low frequency suppression of the conductivity in the normal (neither superconducting or pseudogap) state discussed in section III and shown in Fig 2. However this distinct signature is not apparent in the experimental plots of the normal state conductivity. There are two possibilities: either the scale is very high or the effect is masked by phonons.

A second, generally valid qualitative result is that the simple factor of two relation between ρ_s and the change with onset of phase coherence in the $\omega > 0$ oscillator strength which was found for single-layer systems, no longer applies for bilayer systems (cf Eq 25 and Fig 8); the change in ρ_s is generically greater. This qualitative

behavior has been observed.

A third important result is that the convergence of sum-rule integrals with frequency can be very slow; so caution should be exercised in applying sum-rule arguments to data.

Further we showed that the coupling of phonons, phase fluctuations and the bilayer plasmon leads to complicated effects on the spectrum, which depend sensitively on parameters suggesting that an unambiguous extraction of the bilayer plasmon frequency and spectral weight may be difficult. This is unfortunate, as these quantities in principle carry information about the physically crucial phase fluctuation properties encoded in the Debye-Waller parameter α . We suggest however how the change in conductivity with increasing phase fluctuations (or increasing temperature) is expected to be different based on whether the phonon frequency is above or below the bilayer plasmon frequency.

Acknowledgement: This work was supported in part by NSF-DMR-00081075 and stemmed from a crucial remark of L. B. Ioffe, whose advice and insight we gratefully acknowledge. AJM thanks L. B. Ioffe, S. Das Sarma and D. van der Marel (who pointed out an error in a previous version) for helpful conversations and the Institute for Theoretical Physics and Brookhaven National Laboratories for hospitality and support.

[1] Y. F. Yan, J. M. Harris, N. P. Ong, *Physica C*, **235-240**,

- 1527 (1994); Y. F. Yan et al., *Phys. Rev. B* **52**, R751 (1995).
- [2] C. C. Homes, T. Timusk, D. A. Bonn, R. Liang and W. N. Hardy, *Physica C* **254**, 265 (1995).
- [3] Gruninger M, van der Marel D, Tsverkov AA, Erb A. , *Phys. Rev. Lett.* **84**, 1575 (2000).
- [4] D. N. Basov et al., *Phys. Rev. B* **50**, 3511 (1994); *Phys. Rev. Lett.* **77**, 4090 (1996); A. S. Katz et al., *Phys. Rev. B* **61**, 5930 (2000).
- [5] A. V. Puchkov, D. N. Basov, T. Timusk, *Journal of Physics - Condensed Matter* **8**, 10049-82 (1996).
- [6] P. W. Anderson, *Phys. Rev. Lett.* **67** 3844 (1991).
- [7] P. W. Anderson, *The theory of Superconductivity in the High- T_c Cuprates*, Princeton University Press (Princeton, NJ: 1997).
- [8] D. G. Clarke, S. P. Strong and P. W. Anderson *Phys. Rev. Lett.* **74**, 4499 (1995).
- [9] S. Chakravarty and P. W. Anderson, *Phys. Rev. Lett.* **72**, 3859 (1994).
- [10] S. Das Sarma and E. H. Hwang, *Phys. Rev. Lett.* **81**, 4216 (1998), *Phys. Rev. Lett.* **80**, 4753 (1998).
- [11] M. Tinkham, *Introduction to Superconductivity* (McGraw-Hill, New York, 1996).
- [12] A. J. Millis and L. B. Ioffe, *Science* **285**, 1241-44 (1999).
- [13] L. B. Ioffe and A. J. Millis, *Phys. Rev. B* **61**, 9077 (2000).
- [14] D. Dulic et al., *Phys. Rev. Lett.* **86**, 4144 (2001).
- [15] A. Lopatin, A. Georges and T. Giamarchi, unpublished (cond-mat/0008066).
- [16] A. J. Millis and A. J. Schofield, unpublished
- [17] A. J. Millis, L. B. Ioffe, S. Das Sarma and E. H. Hwang, unpublished.
- [18] W. Kohn, *Phys. Rev.* **133**, A171 (1964).
- [19] M. R. Norman et. al., *et al Nature*, **392**, 157 (1998).
- [20] A. V. Chubukov, *Europhysics Letters*, **44**, 655 (1998); A. V. Chubukov and D. K. Morr, *Phys. Rev. Lett.*, **81**, 471 (1998).
- [21] Z. X. Shen and D. Dessau, *Physics Reports* **253**, 1 (1995).